Effect of Stacking Interactions on the Spectra of the Monomer of PFBT: A Theoretical Study

Jing Wang,[†] Jiande Gu,*[,†,‡] and Jerzy Leszczynski*[,†]

Interdisciplinary Nanotoxicity Center, Department of Chemistry, Jackson State University, Jackson, Mississippi 39217, and Drug Design & Discovery Center, State Key Laboratory of Drug Research, Shanghai Institute of Materia Medica, Shanghai Institutes for Biological Sciences, Chinese Academy of Sciences, Shanghai 201203, P. R. China

Received: April 6, 2009; Revised Manuscript Received: July 21, 2009

Conjugated polymers (CPs) contain one π-conjugated backbone and functional groups that could be ionized in high dielectric media. These materials combine the semiconducting and photon harvesting properties of electronically delocalized polymers with the charge-mediated behavior of polyelectrolytes. CPs can be used as highly responsive optical sensors for chemical and biological targets. The density functional theory (DFT) and the time-dependent density functional theory (TDDFT) approach were employed to simulate the absorption and emission spectra of poly[9,9′-bis(6″-*N*,*N*,*N*-trimethylammonium)hexyl]fluorene-co-alt-4,7-(2,1,3-benzothiadiazole) dibromide] (PFBT) in the present study. The influences on the spectra of the monomer unit F(BT)F due to stacking with the fluorene (F) and 2,1,3-benzothiadiazole (BT) units have been explored. The results suggest that stacking lowers the excitation and emission energy, facilitating detections of the polymers.

1. Introduction

Conjugated polymers (CPs) are constructed by one π-conjugated backbone with functional groups that may ionize in high dielectric media. Water-soluble CPs are suitable for collective response and optical amplification of fluorescent signals.[1,2] Because of the charge-mediated behavior of polyelectrolytes, CPs that form electronically delocalized polymers exhibit semiconducting features and photon harvesting properties.[3,4] CPs have been frequently applied in biosensor designs. One example is the sensory assays of poly[9,9′-bis(6″-*N*,*N*,*N*-trimethylammonium)hexyl]fluorene-co-alt-4,7-(2,1,3-benzothiadiazole) dibromide] (PFBT), which has been designed and incorporated into DNA chips and microarrays for the strand-specific DNA detection.[5] Single nucleotide polymorphism (SNP) can be determined by biosensors that consists of peptide nucleic acid (PNA) probes, an optically amplifying conjugated polymer (CP), and an enzyme named S1 nuclease.[6]

The emission color and electronic properties of CPs are controlled by their molecular structures. The optoelectronic properties of the conjugated polymers of PFBT could be altered by replacing different counterions of the parent conjugated backbone. The X-ray photoelectron spectroscopy experiments reveal that an increase in the size of the counteranion (CA) leads to decreasing the interchain contacts and aggregation. This phenomenon causes a substantial increase in photoluminescence (PL) quantum yields in the bulk. In this way, CPs can be fine-tuned for specific applications.[7]

In the study of four CPs with different counterions and charges on the identical poly(fluorene-*co*-phenylene) backbones, the electronic properties were measured by the absorption and ultraviolet photoelectron spectroscopy (UPS). The results show that these CPs have different molecular orbital energy levels, different ionization potentials (I_p), and different electron affinities (E_A).[8] The interpolyelectrolyte complexes of conjugated copolymers and DNA were explored for the development of multicolor biosensors.[9] One of nonlinear cationic CPs (CCPs) with a range of backbone regiochemistries was synthesized and the fluorescence resonance energy transfer (FRET) experiments indicate that flexible structural polymers are good donors to fluorescein-labeled double-stranded DNA (dsDNA).[10] The excitation process in which FRET transferred from a CCP to an intercalated DNA dye was also investigated. The obtained results show that fluorescein attached at a DNA terminus plays the role as a fluorescence resonance gate for transferring conjugated polymer excitations to dyes intercalated within dsDNA.[11] A self-assembled complex containing a CCP and a dsDNA shows a two-step fluorescence resonance energy-transfer process as detected using pump-dump-emission spectroscopy and time-correlated single-photon counting.[12] Meanwhile, the monomer of PFBT was studied by the time-dependent density functional theory (TDDFT). This theoretical study indicates that the torsion angles between the fluorene and benzothiadiazole units of the CCP PFBT-X may influence both the spatial occupancy and electronic properties of PFBT.[13]

The π-delocalized backbone containing phenylenefluorene segments can be copolymerized with 2,1,3-benzothiadiazole (BT) units and charged pendant groups. Cationic conjugated polyelectrolytes were subsequently designed, synthesized, and characterized to determine the concentrations of dsDNA.[14] However, the mixture of various conjugated polymer nanoparticles (including the blue-emitting polyfluorene (PF) doped with three different green-, yellow-, and red-emitting conjugated polymer acceptors) shows no aggregate features and little improvements in fluorescence quantum yield in the energy-transfer-mediated fluorescence measurement.[15]

Applying the TD-B3LYP approaches, our previous theoretical study on the absorption and emission spectra of the monomer of PFBT provides indication that the TDDFT method with the moderate basis sets (6-311G(d,p) or 6-311++G(d,p)) represents

* Corresponding author. E-mail: jiandegush@go.com (J.G.); jerzy@icnanotox.org. (J.L.).
[†] Jackson State University.
[‡] Chinese Academy of Sciences.

10.1021/jp903168c CCC: $40.75
Published on Web 08/27/2009

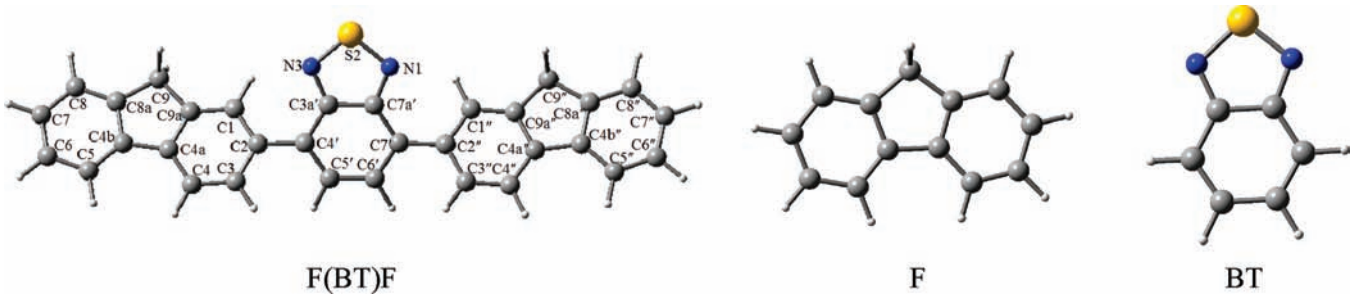

Figure 1. Structure illustrations for monomers of 9,9′-bis-(6′-N,N,N-trimethylammonium)hexyl] fluorene-alt-4,7-(2,1,3-benzothiadiazole) (F(BT)F), fluorene (F), and 2,1,3-benzothiadiazole (BT) (carbon in gray, hydrogen in white, nitrogen in blue, and sulfur in yellow).

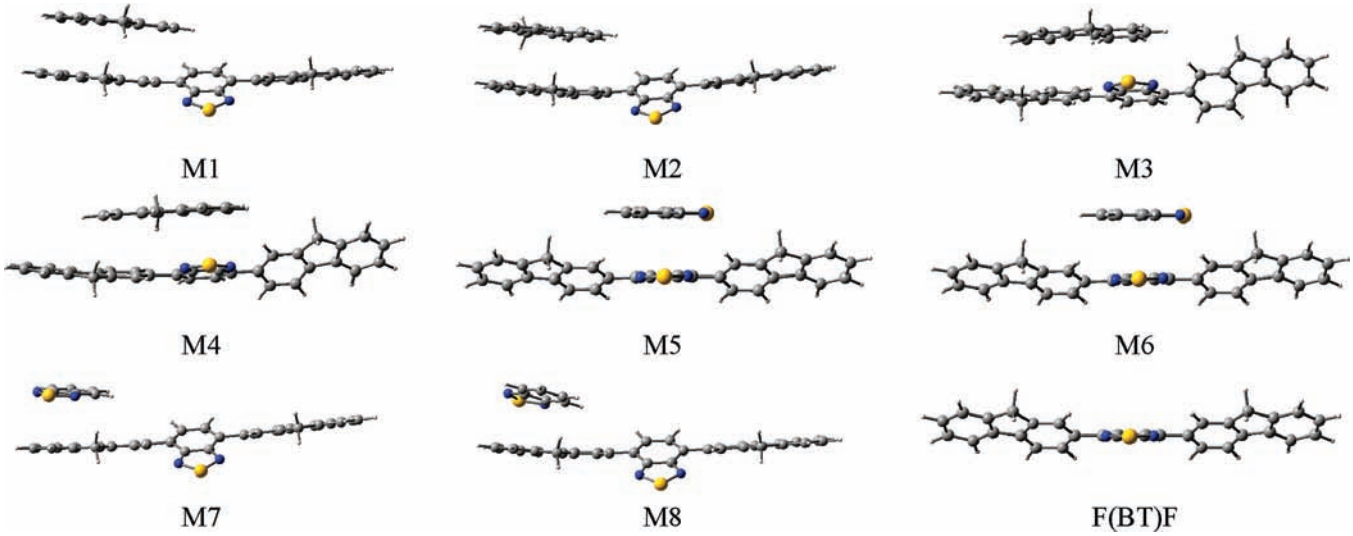

Figure 2. Optimized structures of monomer F(BT)F and the stacked models in their ground states (side view).

reasonable approximation for the investigation of the excitation of the studied systems.[16] Although monomers exhibit intrinsic characteristics of polymers, it is also important to understand their collective behavior. In this paper, we report a TDDFT study of the optical properties of the aggregated polymers considering also the influences of the stacking of the fluorene (F) and 2,1,3-benzothiadiazole (BT) units of the monomer of FBTF (Figure 1).

2. Computational Details

The geometries of the ground state of the stacked monomer/fragment systems shown in Figure 2 have been fully optimized by analytical gradient techniques and the local minimum energy structures are found by ascertaining that all of the harmonic frequencies are real. The density functional theory (DFT) with hybrid BHandH functional was employed which consists of half of the exact (E_x^{HF}) and half of the local spin density approximation (E_x^{LSDA}) for the exchange energy, along with the Lee−Yang−Parr (LYP) nonlocal correlation functional for the correlation energy.[17] The BHandH functional has been reported to represent a reliable theory for stacking descriptions.[18−21] The standard valence triple-ζ basis set, augmented with *d*-type polarization functions for heavy elements and *p*-type polarization functions for H, namely 6-311G(*d*,*p*),[22] was used. It is well-known that the basis set superposition error (BSSE) may overestimate the binding energy of the stacked species. Although the BSSE should be zero as long as the complete basis set is used, the smaller, computationally efficient basis set 6-311G(*d*,*p*) was applied in this study. To improve the reliability of the energy properties of the stacked complexes, we have taken BSSE in binding energies into account through the counterpoise correction of Boys and Bernardi.[23] Clearly, the BSSE provides the up limit of the error because of the insufficient use of the basis set.

Because of the remarkably low computational cost and the accuracy of sophisticated quantum chemical methods for the valence-excited states by the time-dependent density functional theory (TDDFT) method,[24−26] TDDFT has become widely applied in investigations of electronic transition., It is also employed in the present study to predict the electronic vertical singlet transition energies of the studied species at the TD-BHandH/6-311G(d,p) level based on the optimized ground-state geometries. All the calculations were carried out using the Gaussian 03[27] package of programs.

3. Results and Discussion

The optical properties of the monomer of PFBT were explored previously in our laboratory by using the time-dependent DFT approach.[16] This study reveals that the electronic excitation to the lowest singlet $\pi\pi^*$ excited states (S1($\pi\pi^*$)) of FBT is determined mainly by the HOMO−LUMO orbital configuration. To further explore the influence of stacking effects on the spectra of PFBT, we have adopted the fragment units fluorene (F), 2,1,3-benzothiadiazole (BT), and the simplified monomer unit [9,9′-bis-(6′-*N*,*N*,*N*-trimethylammonium)hexyl] fluorene-alt-4,7-(2,1,3-benzothiadiazole) (F(BT)F) as models for the current study (Figure 1).

Among all the possible stacking arrangements, eight stacking patterns were selected (Figure 2). The involving fragment fluorene (F) can be stacked upon F(BT)F either above its

TABLE 1: Geometry and the Absorption Spectra Properties of the Ground State Stacked Models (BHandH/6-311G(d,p) level)

models	*d* (Å)[a]	α (deg)[b]	D1 (deg)[c]	D2 (deg)[d]	Δ*E* (kcal/mol)[e]	$E_{excitation}$(eV)[f]	oscillator strengths (f)	wavelength (nm)
F(BT)F	N/A	N/A	33.1	–33.1	N/A	3.20	0.87	387
M1	3.279	1.8	29.2	–32.8	–10.2 (–7.2)	3.14	0.82	395
M2	3.262	1.5	34.9	–32.8	–11.1 (–8.4)	3.18	0.85	390
M3	3.228	4.4	–24.3	–33.9	–14.2 (–10.1)	3.13	0.75	396
M4	3.286	6.6	–14.6	–32.7	–13.5 (–9.5)	3.06	0.72	406
M5	3.267	1.8	28.0	–34.2	–11.5 (–7.9)	3.13	0.68	396
M6	3.268	1.9	28.0	–34.1	–11.5 (–8.0)	3.13	0.68	396
M7	3.176	7.5	32.7	–33.3	–9.7 (–7.0)	3.18	0.89	390
M8	3.038	14.3	33.3	–32.6	–9.8 (–7.0)	3.19	0.88	389

[a] Distance of the two layers. [b] Dihedral angles of the planes. [c] Dihedral angle of C3a′C4′C2C1 in F(BT)F. [d] Dihedral angle of C7a′C7′C2′C1′ in F(BT)F. [e] Stacking energy of the models and the values in the parentheses are the stacking energies after the basis set superposition error (BSSE) corrections. [f] The excitation energy of the models for the lowest excitation transition.

fluorene (F) segment or above its 2,1,3-benzothiadiazole (BT) segment with parallel and antiparallel reverse displacement. In the former case, two models were constructed for F(BT)F-FF (labeled as M1) and F(BT)F-FF-R (labeled as M2). The other two models constructed by F(BT)F and F unit are M3 (F(BT)F-F(BT)) and M4 (F(BT)F-F(BT)-R). Similar stacking patterns were adopted for the 2,1,3-benzothiadiazole (BT) fragment. Four corresponding stacked complexes are represented by F(BT)F-(BT)(BT), F(BT)F-(BT)(BT)-R, F(BT)F-(BT)F, and F(BT)F-(BT)F-R (denoted as M5, M6, M7 and M8, respectively).

3.1. Ground-State Geometries of the Stacked Complexes. The monomer of F(BT)F and all the eight stacking models were fully optimized in their ground states at the BHandH/6-311G(d,p) level. The optimized structures are shown in Figure 2.

To characterize the stacking features, the distance (d) between the two stacked molecules is defined as the distance from the center of the mass of the segment F (or BT) of the monomer F(BT)F to the average plane of the stacking unit (F or (BT)), where the average plane is defined as a plane through the center of mass perpendicular to the tertiary axis of F or BT. The dihedral angle of two layers is defined as angle α between the vector perpendicular to the plane F (or (BT)) and the vector perpendicular to the plane of F(BT)F. The smaller the dihedral angle α, the more parallel stacked the models are. The BSSE for the studied complexes ranges from 3 to 4 kcal/mol, suggesting that the basis set, 6-311G(d,p), is acceptable for the present study.

The optimized geometry of F(BT)F in the ground state has a symmetric F fragment structure on both sides of the center of BT segment. The bending of F segment toward the BT center is similar at both sides. The dihedral angles for D1(C3a′C4′C2C1) and D2(C7a′C7′C2′C1′) are 33.1 and −33.1°, respectively. The distance between the stacked layers predicted for M1 is 3.28 Å (Table 1). The dihedral angle α between the two planes of monomer F and the unit F of F(BT)F amounts to 1.8°, two molecular planes are nearly parallel to each other. The stacking energy of M1 is predicted to be −10.2 kcal/mol (−7.2 kcal/mol after the BSSE correction, Table 1). Compared with the monomer, the structure of the F(BT)F of M1 changes slightly. The dihedral angle D1 is 29.2° and D2 is −32.8°. The stacking energy of M2 is −11.1 kcal/mol (−8.4 kcal/mol after the BSSE correction), slightly larger (about 1 kcal/mol) than that of M1. Consistently, M2 also has a shorter distance between the two layers (3.26 Å). The dihedral angle of the two layers in M2 is also small (1.5°). These parameters indicate a well-stacked complex. It is interesting that the structure of F(BT)F in M2 is almost the same as that of the monomer (with D1 and D2 as 34.9 and −32.8°). This suggests that the influence of this stacking pattern of the F unit on the geometry of the monomer is insignificant.

The distance between the two layers of M3 is 3.23 Å, whereas that of antiparallel stacked M4 is 3.29 Å. The dihedral angles α are 4.4 and 6.6° for M3 and M4, respectively, which suggest a slightly more twisted stacking pattern for M3 and M4 when compared to M1 and M2. The dihedral angles D2 of F(BT)F layer in M3 and M4 are predicted to be similar to that of the monomer F(BT)F. The dihedral angle D1 displays a notable change compared to the monomer (33.1°), where D1 of M3 amounts to −24.3° while D1 in M4 is −14.6°. It suggests that one of the F segment becomes more planar with the BT plane within the F(BT)F layer and the overlapping area of F(BT)F by F in M3 and M4 is larger than that of M1 and M2. Such geometry implies a better stacking pattern for M3 and M4 characterized by larger stacking energies (−14.2 and −13.5 kcal/mol).

M5 and M6 consist of a BT unit stacked upon the BT segment of F(BT)F. Although BT in M5 is stacked with F(BT)F in a different pattern from that in M6 (parallel vs antiparallel), both M5 and M6 reveal the same interlayer distance (3.3 Å) and the same interplane angle (α = 2°). The stacking energies of M5 and M6 are also close (−11.5 kcal/mol for both). On the other hand, the stacking over the BT moiety of F(BT)F decreases the dihedral angles of D1 (28°) but increases D2 (−34°) in F(BT)F. When BT unit stacks over the F segment of F(BT)F (M7 and M8), the distance between the stacked layers is closer. The interlayer distances are 3.18 Å for M7 and 3.04 Å for M8. However, compared to M5 and M6, the angle between the stacked layers is larger in M7 and M8 (7.5° for M7 and 14.3° for M8). The tilted stacking of M7 and M8 is in accordance with the smaller stacking energy (−9.7 kcal/mol for M7 and −9.8 kcal/mol for M8). In the case of stacking interactions, the larger plane−plane angle of M8 (14.3°) is compensated by the shorter interlayer distance (3.04 Å). The directions of BT adopted in the stacked models (parallel in M7 and antiparallel in M8) affect the stacking energy insignificantly. With a different stacking pattern from M5 and M6 (BT stacks over the BT moiety), the dihedral angles D1 and D2 of F(BT)F in M7 and M8 are unaffected by the stacking of BT over its F moiety.

It can be seen that the stacking has more pronounced parallel arrangement when the stacking occurs between the same fragment (M1, M2, M5, and M6). The dihedral angles α of these four models are less than 2°. Among the eight stacking models, when compared to the F(BT)F monomer, M3 and M4 have a different layer structure of F(BT)F while the other six models keep the geometry the same as that of the monomer.

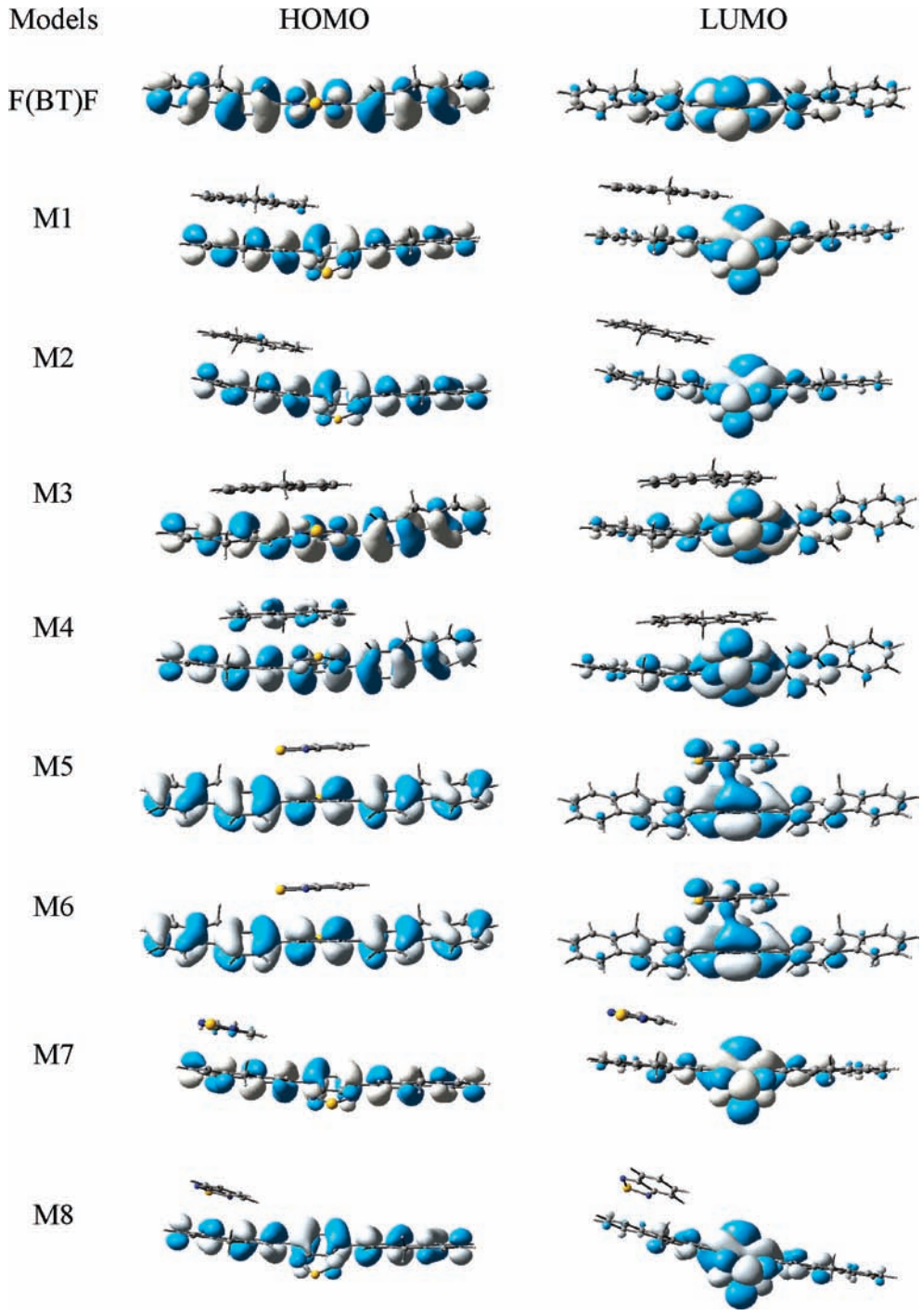

Figure 3. HOMO and LUMO molecular orbitals of monomer F(BT)F and the stacked models.

3.2. Vertical Singlet Transition Energies of the Stacked Models. For the monomer of F(BT)F and all the eight stacked models, the optimized reference geometries were used to calculate the electronic vertical singlet excitation energies at the TD-BHandH/6-311G(d,p) level.

On the basis of the optimized geometry of the ground state, the dominant absorption band of the studied species is found to be associated with the first excited state (with oscillator strength more than 0.68) and all the other higher energy states are characterized by much smaller oscillator strengths (less than 0.01). Typical π type molecular orbital characteristics are observed in all the highest occupied molecular orbitals (HOMO) and the lowest unoccupied molecular orbitals (LUMO) (Figure 3). Similar to the excitation of the monomer of PFBT,[16] for the present stacked models, the electronic excitation to the lowest singlet $\pi\pi^*$ excited state (S1($\pi\pi^*$)) is also dominated by HOMO → LUMO transition.

As listed in Table 1, the F(BT)F monomer is characterized by the excitation energy 3.20 eV (387 nm) with the oscillator strength of 0.87 for the lowest excitation transition. The HOMO extends essentially over the F and BT part, but the LUMO locates mainly on the BT segment (Figure 3). The intramolecular charge transfer is hence to be connected with this excitation for the considered single layer model, which is consistent with the conclusion of our previous study.[16] The parallel stacking model M1 has the lowest excitation transition 3.14 eV (395 nm) above the ground state, which is 0.06 eV lower in excitation energy and 8 nm shorter in maximum excitation wavelength

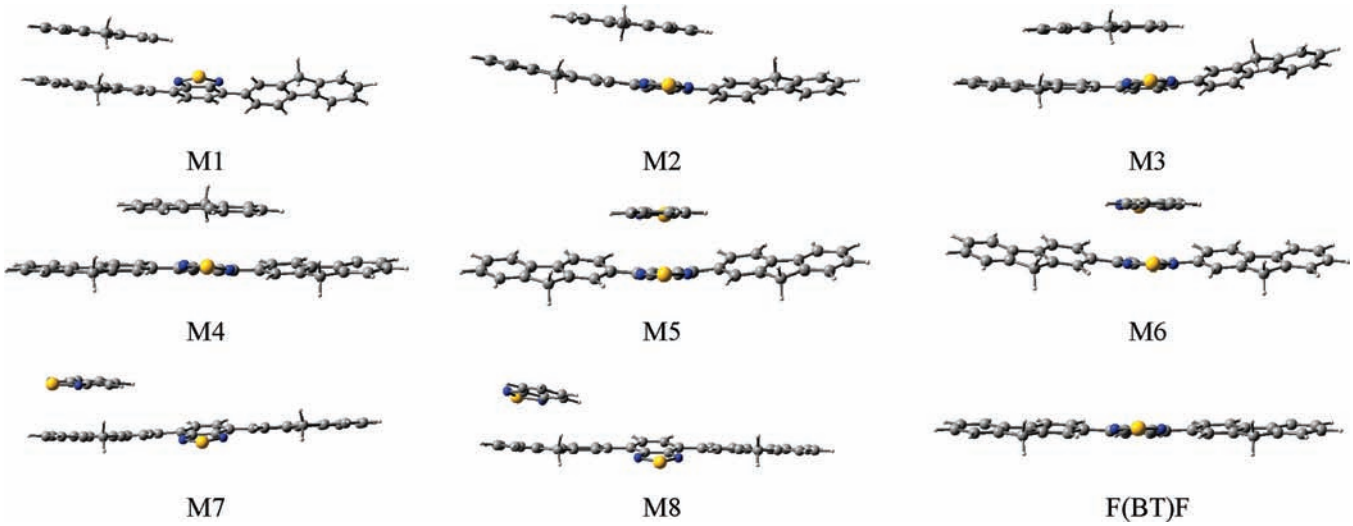

Figure 4. Optimized structures of monomer F(BT)F and the stacked models in their triplet states (side view).

than the corresponding characteristics of the monomer. The stacked M1 reveals similar electron distribution for HOMO and LUMO as those of the F(BT)F monomer. The HOMO of M1 displays an even distribution on the layer of F(BT)F, whereas the upper stacking unit of F is almost empty. On the other hand, the LUMO of M1 illustrates the electron distribution focusing on the center part (BT) of the F(BT)F layer that is the same as in the monomer.

The related antiparallel stacking model M2 shows no major differences in the optical parameters and the HOMO//LUMO features with those of M1. The lowest excitation transition energy of M2 is calculated to be 3.18 eV (0.04 eV higher than that of M1) and is only 3 nm red-shifted from the maximum excitation wavelength of the monomer.

As discussed in the previous section, M3 and M4 geometries demonstrate a significant change in the structure of the F(BT)F layer. They are also characterized by a stronger stacking energy. Besides, M3 has a lower excitation energy (3.13 eV) and M4 reveals the lowest excitation energy of 3.06 eV, which leads to a nearly 20 nm red-shifted maximum excitation wavelength when compared to that of the monomer. It should be mentioned that although the LUMO of M4 is similar to that of the monomer, the HOMO of M4 has the electron distribution mainly on the F(BT)F layer and partly on the stacking F layer.

The M5 and M6 models have similar stacking geometry features which lead to the similar optical properties. The excitation energy of the lowest excitation is calculated to be 3.13 eV for both systems. The HOMO reveals the similar distribution as M1, which means the electron distribution is on the F(BT)F layer and little is shown for the BT layer. However, the LUMO reveals that the distribution extends not only upon the BT segment of the F(BT)F layer, but also partly overlaps with the BT layer.

As mentioned above, M7 and M8 demonstrate the most twisted stacking patterns, which suggests that the effects of the stacking should be observed at least on the optical properties of F(BT)F. Consistently, the excitation energy for these two complexes is around 3.2 eV. The red-shifting for M7 and M8 is less than 3 nm. The HOMO and LUMO distributions show little differences with those of M1 and M2.

It can be concluded that stacking of F or BT unit on the layer of F(BT)F will facilitate excitation by lowering the excitation energy by 0.1−0.14 eV and the maximum excitation wavelength therefore is red-shifted by 2−19 nm. Generally, more pronounced stacking patterns have more influences on the spectra of F(BT)F.

3.3. Emission Properties of the Stacked Models. Our previous study[16] suggests that it is reasonable to apply the fully optimized triplet state structure to approximate the local minimum structure of the open-shell singlet first-excited state. We applied the same approximations to study the emission spectra for the F(BT)F monomer and the eight stacking models.

All the geometries of the studied models have been further fully optimized in their triplet state at BHandH/6-311G(d,p) level (Figure 4). The relative emission spectra are predicted through the TD-BHandH method based on the optimized structure of the first excited state.

The optimized monomer F(BT)F in triplet state shows a more planar structure than that in ground state. The dihedral angles of D1 and D2 (Table 2) are by about 20° different from those in the ground state structure (13 vs 33° and −13 vs −33°, respectively). The figures of the two singly occupied molecular orbitals (SOMO1 and SOMO2) of the excited state of F(BT)F (Figure 5) display the typical π type features of the molecular orbitals. The SOMO2 indicates the partial migration of the electron distribution from BT center to F units. The lowest emission energy is calculated to be 2.29 eV, which is 0.91 eV lower than the lowest excitation energy.

The molecular structure of M1 in triplet state shows a closer stacking pattern due to the fact that the distance between the two layers is reduced to 3.25 Å and the dihedral angle α (2.1°) suggests that M1 is also well-stacked in its triplet state. Meanwhile, the values of dihedral angles D1 and D2 (−15.4 and −13.1°) illustrate a more planar layer of F(BT)F. The SOMO1 shows the electron spreading mostly upon the F(BT)F layer and slightly over the F layer. Another way of density distribution is observed for the SOMO2, which has the localized distribution on the BT center area of the F(BT)F layer. The emission energy of M1 amounts to 2.23 eV, which is 0.06 eV lower than that of monomer F(BT)F. Nevertheless, the relative antiparallel stacked M2 model is more densely packed. The distance between the planes amounts to 3.1 Å, which is more than 0.16 Å shorter than that of M1. The SOMO1 and SOMO2 of M2 are similar to those of M1. The maximum emission wavelength of M2 amounts to 564 nm, which is red-shifted by 21 nm compared to monomer F(BT)F.

TABLE 2: Geometry and the Emission Spectra Properties of the Triplet State Stacked Models (BHandH/6-311G(d,p) level)

models	*d* (Å)[a]	α (deg)[b]	D1 (deg)[c]	D2 (deg)[d]	$E_{emission}$(eV)[e]	oscillator strengths (f)	wavelength (nm)
F(BT)F	N/A	N/A	13.0	–13.0	2.29	0.91	543
M1	3.254	2.1	–15.4	–13.1	2.23	0.86	557
M2	3.093	5.0	–14.5	–4.1	2.20	0.69	564
M3	3.202	3.5	–13.2	–10.4	2.21	0.69	562
M4	3.067	8.3	–7.3	12.0	2.14	0.63	579
M5	3.215	2.7	21.8	–20.5	2.23	0.68	555
M6	3.214	2.7	20.4	–21.7	2.23	0.68	555
M7	3.183	5.4	11.1	–13.2	2.26	0.95	548
M8	3.053	13.8	12.4	–13.1	2.27	0.93	546

[a] Distance of the two layers. [b] Dihedral angles of the planes. [c] Dihedral angle of C3a′C4′C2C1 in F(BT)F. [d] Dihedral angle of C7a′C7′C2′C1′ in F(BT)F. [e] The emission energy of the models for the lowest excitation transition.

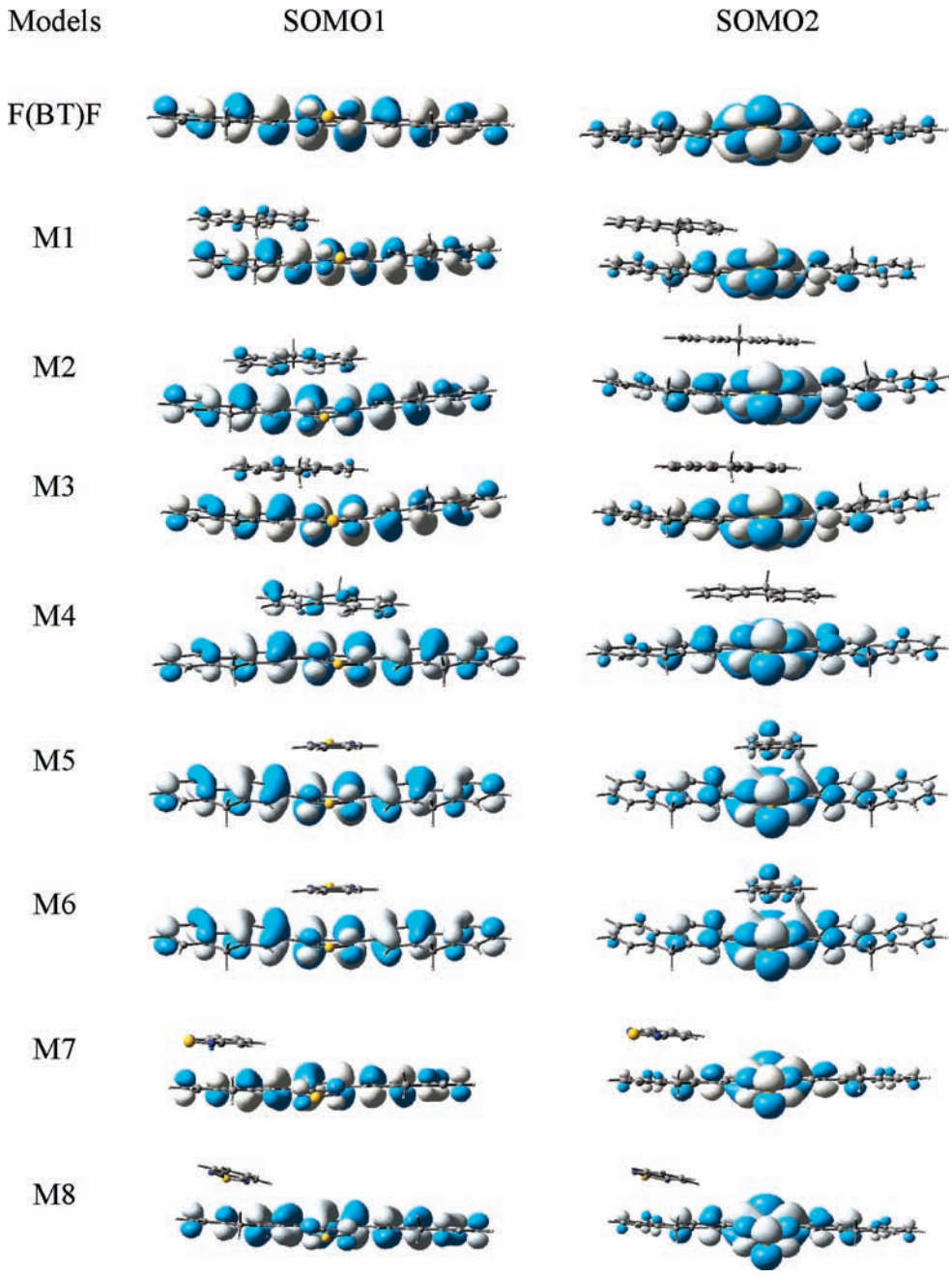

Figure 5. SOMO1 and SOMO2 molecular orbitals of monomer F(BT)F and the stacked models.

The features of M3 in triplet state are approximately the same as those predicted for M1. M3 has the emission energy as 2.21 eV. It should be noted that the structure of M4 in triplet state shows a dramatic change in the stacking. The distance between the planes is 0.22 Å shorter than for the ground state structure. The dihedral angles D1 and D2 are predicted to be 12.0° and

−13.2°. The emission energy of M4 is the lowest among all the considered models (2.14 eV) and the emission wavelength reaches 579 nm (36 nm red-shifted compared with monomer F(BT)F). Both M5 and M6 models illustrate a closer stacking by 0.05 Å in their triplet state, where the emission energy is estimated to be 2.23 eV.

M7 and M8 still retain a more pronounced twisted stacking pattern than the other species in their triplet state with the dihedral angle α of the planes that amounts to 5.4 and 13.8°. Their emission energy is predicted to be 2.3 eV with stronger oscillator strength (0.9).

For all the studies models, both the monomer F(BT)F and the F(BT)F layer in the stacking complexes appear to be more planar in their triplet state than in their ground state. Generally, the stacking upon the monomer F(BT)F contributes toward lowering the emission energy. Different stacking patterns have various effects on the spectra.

Also, it is very important to note that the lowest singlet transitions of the stacked dimers have partial charge transfer (CT) character. This is clear from visualization of the MOs (especially for M4, M5, and M6) displayed in Figures 3 and 5. A pure local exchange-correlation functional may underestimate the charge transfer transition energies as it does not properly account for the Coulombic interaction in the excited states. Hybrid functionals that include exact HF exchange improve the asymptotic behavior of the excitation energy of a CT state within the TDDFT. Comparatively large HF exchange contribution in the "half and half" functional of BHandH that has been employed in this study may help to overcome the problem of low-lying spurious CT states.[26,28]

4. Conclusions

The molecular structures and the optical properties of the F(BT)F monomer and eight stacked models have been theoretically explored at the BHandH/6-311G(d,p)//TD-BHandH/6-311G(d,p) level. The electronic excitation to the lowest singlet $\pi\pi^*$ excited state (S1($\pi\pi^*$)) of all models is dominated by the HOMO → LUMO orbital configuration. Our study illustrates that the stacking of F or BT units upon the monomer F(BT)F can lower the absorption and emission energy of F(BT)F. It can be expected that the aggregation of the CP polymers facilitates detections of these species. Enhanced stacking has more pronounced effects on the spectra of the polymer.

Acknowledgment. This work was financially supported by the NSF-PREM program (Grant 0611539). We thank the Mississippi Center for Supercomputing Research for a generous allotment of computer time.

References and Notes

(1) Wilson, W. D. *Science* **2002**, *295*, 2103–2105.
(2) Aldaz-carroll, L.; Tallet, B.; Dausse, E.; Yurchenko, L.; Toulme, J. J. *Biochemistry* **2002**, *41*, 5883–5893.
(3) Pinto, M. R.; Schanze, K. S. *Synthesis* **2002**, *9*, 1293–1309.
(4) Bazan, G. C. *J. Org. Chem.* **2007**, *72*, 8615–8635.
(5) Liu, B.; Bazan, G. C. *Proc. Natl. Acad. Sci. U.S.A.* **2005**, *102*, 589–593.
(6) Gaylord, B. S.; Massie, M. R.; Feinstein, S. C.; Bazan, G. C. *Proc. Natl. Acad. Sci. U.S.A.* **2005**, *102*, 34–39.
(7) Yang, R.; Garcia, A.; Korystov, D.; Mikhailovsky, A.; Bazan, G. C.; Nguyen, T.-Q. *J. Am. Chem. Soc.* **2006**, *128*, 16532–16539.
(8) Seo, J. H.; Nguyen, T.-Q. *J. Am. Chem. Soc.* **2008**, *130*, 10042–10043.
(9) Liu, B.; Bazan, G. C. *J. Am. Chem. Soc.* **2004**, *126*, 1942–1943.
(10) Liu, B.; Wang, S.; Bazan, G. C.; Mikhailovsky, A. *J. Am. Chem. Soc.* **2003**, *125*, 13306–13307.
(11) Wang, S.; Gaylord, B. S.; Bazan, G. C. *J. Am. Chem. Soc.* **2004**, *126*, 5446–5451.
(12) Xu, Q.-H.; Wang, S.; Korystov, D.; Mikhailovsky, A.; Bazan, G. C.; Moses, D.; Heeger, A. J. *Proc. Natl. Acad. Sci. U.S.A.* **2005**, *102*, 530–535.
(13) Sheng, Y.; Leszczynski, J.; Nguyen, T.-Q.; Bamgbelu, A. *Struct. Chem.* **2007**, *18*, 827–832.
(14) Chi, C.; Mikhailovsky, A.; Bazan, G. C. *J. Am. Chem. Soc.* **2007**, *129*, 11134–11145.
(15) Wu, C.; Peng, H.; Jiang, Y.; Mcneill, J. *J. Phys. Chem. B* **2006**, *110*, 14148–14154.
(16) Wang, J.; Gu, J.; Leszczynski, J. *Chem. Phys. Lett.* **2008**, *456*, 206–210.
(17) Becke, A. D. *J. Chem. Phys.* **1993**, *98*, 1372–1377.
(18) González Moa, M. J.; Mandado, M.; Mosquera, R. A. *J. Phys. Chem. A* **2007**, *111*, 1998–2001.
(19) Gkionis, K.; Platts, J. A.; Hill, J. G. *Inorg. Chem.* **2008**, *47*, 3893–3902.
(20) Robertazzi, A.; Platts, J. A. *J. Phys. Chem. A* **2006**, *110*, 3992–4000.
(21) Waller, M. P.; Robertazzi, A.; Platts, J. A.; Hibbs, D. E.; Williams, P. A. *J. Comput. Chem.* **2006**, *27*, 491–504.
(22) Casida, M. E.; Jamorski, C.; Casida, K. C.; Salahub, D. R. *J. Chem. Phys.* **1998**, *108*, 4439–4449.
(23) Boys, S. F.; Bernardi, F. *Mol. Phys.* **1970**, *19*, 553–566.
(24) Stratmann, R. E.; Scuseria, G. E.; Frisch, M. J. *J. Chem. Phys.* **1998**, *109*, 8218–8224.
(25) Bauernschmitt, R.; Ahlrichs, R. *Chem. Phys. Lett.* **1996**, *256*, 454–464.
(26) Dreuw, A.; Head-Gordon, M. *Chem. Rev.* **2005**, *105*, 4009–4037.
(27) Frisch, M. J.; Trucks, G. W.; Schlegel, H. B.; Gill, P. M. W.; Johnson, B. G.; Robb, M. A.; Cheeseman, J. R.; Keith, T.; Petersson, G. A.; Montgomery, J. A.; Raghavachari, K.; Al-Laham, M. A.; Zakrzewski, V. G.; Ortiz, J. V.; Foresman, J. B.; Cioslowski, J.; Stefanov, B. B.; Nanayakkara, A.; Challacombe, M.; Peng, C. Y.; Ayala, P. Y.; Chen, W.; Wong, M. W.; Andres, J. L.; Replogle, E. S.; Gomperts, R.; Martin, R. L.; Fox, D. J.; Binkley, J. S.; Defrees, D. J.; Baker, J.; Stewart, J. P.; Head-Gordon, M.; Gonzalez, C.; Pople, J. A. *Gaussian 03, revision C.01*; Gaussian, Inc.: Pittsburgh, PA, 2004.
(28) Dreuw, A.; Weisman, J. L.; Head-Gordon, M. *J. Chem. Phys.* **2003**, *119*, 2943–2946.

JP903168C